

Research Paper

HMGA1 Activates FGFBP1 Transcription to Enhance Angiogenesis Induction and Tumor Progression via FGF2/FGFR1 Pathway

Zhe Zhang¹, Yili Xiong^{2,3}, Mingyang Li², Shengyao Wang¹, Zhenxing Liu^{2,3}, Guanduo Wang⁴, Huanqing Zhang⁴, Xiaojuan Yang⁴, Gangli Liu¹✉, Dongsheng Zhang^{2,3}✉, Haiwei Wu^{2,3}✉, Shengyun Huang^{2,3}✉

1. Department of Oral and Maxillofacial Surgery, School and Hospital of Stomatology, Cheeloo College of Medicine, Shandong University & Shandong Key Laboratory of Oral Tissue Regeneration & Shandong Engineering Laboratory for Dental Materials and Oral Tissue Regeneration & Shandong Provincial Clinical Research Center for Oral Diseases, Jinan, Shandong, 250012, China.
2. Department of Oral and Maxillofacial Surgery, Shandong Provincial Hospital Affiliated to Shandong First Medical University, Jinan, Shandong, 250021, China.
3. School of Stomatology, Shandong First Medical University, Jinan, Shandong, 250117, China.
4. Department of Oral and Maxillofacial Surgery, Shandong Provincial Hospital, Cheeloo College of Medicine, Shandong University, Jinan, Shandong, 250021, China.

✉ Corresponding authors: Gangli Liu (liugangli@sdu.edu.cn); Dongsheng Zhang (ds63zhang@sdu.edu.cn); Haiwei Wu (hwwu@sdfmu.edu.cn); Shengyun Huang (huangsy28@163.com, Tel: +86 15853199111).

© The author(s). This is an open access article distributed under the terms of the Creative Commons Attribution License (<https://creativecommons.org/licenses/by/4.0/>). See <https://ivyspring.com/terms> for full terms and conditions.

Received: 2024.12.19; Accepted: 2026.02.13; Published: 2026.02.26

Abstract

High mobility group AT-hook 1 (HMGA1) is a chromatin regulator overexpressed in various cancers, often predicting poor outcomes. However, its role in head and neck squamous cell carcinoma (HNSCC) remains unclear. A hallmark of HNSCC is the rapid growth of its vasculature. Here, we identify an epigenetic mechanism whereby HMGA1 promotes tumor progression and angiogenesis via upregulation of fibroblast growth factor-binding protein 1 (FGFBP1). *HMGA1* silencing suppressed oncogenic properties *in vitro* and reduced tumor initiating cells in HNSCC xenograft mice. RNA sequencing revealed that HMGA1 regulated transcriptional networks involved in tumor progression and angiogenesis, including the *FGFBP1* gene. HMGA1 directly binds to the *FGFBP1* promoter to induce its expression. This upregulation increased secretion of FGFBP1's target, FGF2. Interestingly, disrupting FGFBP1 via gene silencing or the FGFR1 inhibitor PD166866 recapitulated phenotypes observed with *HMGA1* silencing. Blocking *HMGA1*, *FGFBP1*, or FGFR1 also reduced stromal formation and increased tumor necrosis. In human HNSCC, the combined analysis of HMGA1 and FGFBP1 provides a more detailed evaluation of patient prognosis. Our findings highlight a novel paradigm where HMGA1 and FGFBP1 drive tumor progression and angiogenesis, presenting them as potential therapeutic targets for HNSCC.

Keywords: HMGA1, FGFBP1, FGF2, FGFR1, Transcription, Angiogenesis

Background

Head and neck squamous cell carcinoma (HNSCC) accounts for about 90% of head and neck malignancies, with poor prognosis and low five-year survival rate, making it a significant public health issue [1]. Standard treatments, such as surgery, radiotherapy, chemotherapy, and immunotherapy, offer limited survival improvements, necessitating novel therapeutic approaches [2].

Angiogenesis is one of the hallmarks of HNSCC. Both HNSCC cells and stromal cells produce a variety

of pro-angiogenic factors, which activate endothelial cells and induce angiogenesis, serving as a key driver of HNSCC progression [3].

Vascular endothelial growth factor (VEGF) is highly expressed in HNSCC and acts as a pro-angiogenic factor. VEGF and its receptor VEGFR play a dominant role in the angiogenesis system. Multiple inhibitors and other types of drugs targeting VEGF/VEGFR have been approved by the FDA for HNSCC treatment, and numerous drugs are

undergoing clinical trials [4]. Results from clinical studies over the past 5 years indicate that their combination with chemotherapy, targeted therapy, and immunotherapy enhances the efficacy of these treatments in HNSCC [5–8]. This demonstrates the therapeutic potential of anti-angiogenic therapy in HNSCC.

However, due to the complex mechanisms of tumor angiogenesis, anti-angiogenic therapy still faces several shortcomings, including tumor recurrence, drug resistance, lack of biomarkers, short-term efficacy, and severe adverse events [4]. Therefore, further investigation into the mechanisms of tumor angiogenesis is necessary for the improvement of anti-angiogenic therapies.

Both HNSCC cells and stromal cells, such as cancer-associated fibroblasts and tumor-associated tissue eosinophils, can induce angiogenesis [9–14]. It has been found that HNSCC cells promote angiogenesis through highly expressed phosphofruktokinase-platelet (PFKP) or circular RNA circFNDC3B [9,10]. Additionally, HNSCC cells can secrete TGFβ⁺ small extracellular vesicles to reprogram primary human macrophages into a pro-angiogenic phenotype [11]. This suggests that HNSCC cells can induce angiogenesis through various mechanisms to promote tumor progression. Therefore, studying the mechanisms by which HNSCC cells induce endothelial cell-mediated blood vessel formation is meaningful for a deeper understanding of angiogenesis in HNSCC and may provide new strategies for anti-angiogenic therapy.

Epigenetic regulation, including DNA methylation, histone modifications, chromatin remodeling, and non-coding RNAs, is involved in HNSCC. This can promote the occurrence and development of tumors [15]. Therefore, exploring epigenetic phenomena may help to identify novel therapeutic targets. Chromatin modifiers regulate gene expression by altering chromatin structure [16]. High mobility group AT-hook 1 (HMGA1) is a chromatin modifier highly expressed in stem cells but low in well-differentiated cells [17]. Alternative splicing produces HMGA1a and HMGA1b, which bind to AT-rich DNA regions, open chromatin, and recruit transcriptional regulators and some activated histone modifications, such as acetylated histones [18]. HMGA1 is highly expressed in many cancers, often predicting poor prognosis and differentiation [19–25]. In pancreatic ductal adenocarcinoma and myeloproliferative neoplasms, HMGA1 silencing reduces tumorigenic properties and prolongs survival in mice models [19,20].

In HNSCC, HMGA1 expression correlates with clinical features like grade and lymph metastasis,

though findings vary across studies due to sample and method differences [26–31]. In oral potentially malignant diseases, HMGA1 is elevated and activates myofibroblasts [32,33]. HMGA1 silencing in breast cancer cells reduces the tube formation of human umbilical vein endothelial cells (HUVECs) by downregulating VEGFA [34]. However, its role in HNSCC transcriptional networks and angiogenesis remains unclear.

Our study uncovers a novel role for HMGA1 in HNSCC, showing that it upregulates FGFBP1 to drive angiogenesis and tumor growth. HMGA1 binds to the promoter of fibroblast growth factor-binding protein 1 (*FGFBP1*), enhancing its expression and thereby modulating the fibroblast growth factor 2/ fibroblast growth factor receptor 1 (FGF2/FGFR1) signaling pathway. Silencing *HMGA1* or *FGFBP1* inhibited the oncogenic phenotypes and angiogenesis-inducing ability of HNSCC cells both *in vitro* and *in vivo*. Overexpression of *FGFBP1* or exogenous human FGF2 reversed this effect of *HMGA1* silencing. PD166866, an FGFR1 inhibitor, similarly blocked FGF2 effects, recapitulated the effects of *HMGA1* or *FGFBP1* silencing. High HMGA1 expression correlates with poor prognosis in HNSCC, with subgroups based on HMGA1 and FGFBP1 expression showing differential outcomes. Together, these findings suggest HMGA1/FGFBP1/FGF2/FGFR1 as a promising therapeutic target for HNSCC treatment.

Methods

Bioinformatics analysis

scRNA-seq data were processed using “Seurat 5.0,” filtering cells with 500–6000 UMI counts and excluding those with >10% mitochondrial UMIs, resulting in 53,232 cells. PCA and clustering were performed with the top 50 principal components, and nine major cell types were identified. CNVs in epithelial cells were estimated with InferCNV. DEG analysis was done using the “Limma” package (Adjusted $P < 0.05$, $|\log_2(\text{siHMGA1}/\text{control})| \geq 0.5$), and GO enrichment was conducted using “clusterProfiler.” Hallmark gene sets were analyzed via ssGSEA, and Kaplan–Meier survival analyses were performed with “survminer” and “survival.”

Patient tissue samples

HNSCC tissue samples and matched adjacent non-tumorous tissues were obtained from the Department of Pathology, Shandong Provincial Hospital, collected between May 2023 and March 2024.

Cell lines and culture conditions

HNSCC cell lines (Cal27, HSC2, SCC15, SCC25), normal human oral epithelial cells (HOEC), and human umbilical vein endothelial cells (HUVECs) were used. HSC2 and HOEC were purchased from Otwo Biotech, Cal27 from Procell, SCC15 and SCC25 from ATCC, and HUVECs from Immocell. All cell lines were authenticated and mycoplasma-negative. Cells were cultured in their respective media with 10% FBS and 1% penicillin-streptomycin, under standard conditions at 37°C with 5% CO₂.

Cell transfection with siRNA, shRNA and plasmids

siRNAs and plasmids were synthesized by Genomeditech, and lentiviruses by Genechem. Transfection was performed using GMTrans Liposomal Reagent, followed by RT-qPCR and Western blotting 48 hours post-transfection. Cal27 cells were infected with lentivirus for 16 hours, then selected with puromycin (10 µg/mL) for 72 hours to generate stable clones. Silencing or overexpression efficiency was evaluated by RT-qPCR and Western blotting.

RNA isolation and reverse transcriptase quantitative PCR (RT-qPCR) assay

Total RNA was extracted using the SteadyPure Universal RNA Extraction Kit (Accurate Biology) and cDNA synthesized from 1 µg RNA using the Evo M-MLV RT Mix Kit. RT-qPCR was performed with the 2X SYBR Green Pro Taq HS Premix on the LightCycler 480 system. Gene expression was normalized to β-actin and calculated using the 2^{-ΔΔCt} method.

Western blot

Cells were lysed in RIPA buffer, and protein concentration was measured using the BCA assay. Equal protein amounts were separated by SDS-PAGE, transferred to PVDF membranes, and incubated with primary and secondary antibodies. Protein bands were visualized using ECL and imaged with an Amersham Imager 600. Secreted proteins were concentrated with methanol and chloroform and analyzed by Western blotting to assess FGF2 expression.

Cell proliferation assay

Cell proliferation was assessed using the CCK-8 assay over 4 or 7 days. Cells were seeded in 96-well plates at 3,000 cells per well and incubated at 37°C with 5% CO₂. After treatments, 10 µL of CCK-8 solution was added daily, and absorbance at 450 nm was measured using a ThermoMultiskan GO.

Proliferation data were normalized to the control group absorbance on day 0.

Colony formation assay

Cells were trypsinized, seeded in 6-well plates at 800-1000 cells per well, and cultured for 10-14 days at 37°C with 5% CO₂ until colonies formed. The medium was changed every 3 days. Colonies were fixed with 4% paraformaldehyde, stained with 1% crystal violet, and counted if consisting of 50 or more cells using ImageJ software.

Scratch assay

HNSCC cells were treated with 10 µM Cytosine β-D-arabinofuranoside (Ara-C) for 1 h to inhibit proliferation, and linear scratches were created in 6-well plates with 1% FBS for 20 hours. Migration was assessed by measuring scratch gaps under a microscope.

Transwell migration and Matrigel invasion assays

For migration and invasion assays, HNSCC cells were cultured in serum-free medium for 24 hours and then treated with 10 µM Ara-C for 1 hour. Cells (5×10⁴) were seeded in the upper chambers of Transwell inserts, with Matrigel coating for invasion. After 20 hours of incubation, non-migrating/invasive cells were removed, and those on the lower surface were fixed, stained with crystal violet, washed, and photographed.

In vivo limiting dilution assay

To evaluate tumor-initiating potential, varying cell numbers (1 × 10⁴, 5 × 10⁴, and 1 × 10⁵) were injected into BALB/c nude mice and monitored for 5, 6, and 9 weeks, respectively. Tumor volume was calculated using the formula: volume = 0.5 × length × width² [35]. Tumor-initiating cell frequency was assessed by Extreme Limiting Dilution Analysis (ELDA), with statistical significance determined using the chi-square test [36]. Mice were kept in SPF conditions.

RNA sequencing (RNAseq)

RNA was extracted using RNAex Pro Reagent, and library construction and sequencing were performed by the Beijing Genomics Institute. Data analysis was done using an internal assembler and variant caller. Clean reads were aligned to the reference genome with STAR, and gene read counts were obtained with HTSeq. Differential expression was analyzed using the edgeR package, with genes showing a log₂ fold change ≥ 0.5 and adjusted P < 0.05 considered significantly different (Supplemental

Table 1).

Ethynyl-2-deoxyuridine (EdU) proliferation assay

Cell proliferation in Cal27 cells was assessed using the EdU Apollo DNA Kit. Transfected cells and controls (3×10^3 cells/well) were seeded in 96-well plates and treated with human FGF2 protein. After 72 hours, cells were incubated with 20 μ M EdU for 2 hours, fixed, and stained with Apollo 488 for EdU detection and Hoechst 33342 for nuclear staining. EdU-positive cells were quantified using ImageJ software.

Chromatin immunoprecipitation (ChIP)-quantitative PCR (qPCR) assay

ChIP assays were performed using the Pierce™ Agarose ChIP Kit. Chromatin was cross-linked, sheared, and treated with Micrococcal Nuclease. The FGFBP1 promoter region, predicted to contain an HMGA1 binding site, was amplified using primers designed for a 142 bp product (Supplementary Table 1). After immunoprecipitation, DNA was purified and analyzed by qPCR, with specificity confirmed by gel electrophoresis. Enrichment of the FGFBP1 promoter was calculated relative to a nonspecific IgG control and normalized to input DNA.

Agarose gel electrophoresis

Agarose gel electrophoresis was performed to assess DNA fragmentation and PCR product specificity. A 1.2% agarose gel was prepared with TAE buffer, stained with nucleic acid dye, and loaded with DNA samples mixed with loading buffer. DNA fragments were sized using a DNA ladder and electrophoresed at 120 V. Bands were visualized using a UV transilluminator.

Dual-luciferase reporter assay

The dual-luciferase reporter assay was used to assess HMGA1's transcriptional activation of the FGFBP1 promoter. Cal27 cells were co-transfected with firefly luciferase plasmids (wild-type and mutated FGFBP1 promoter regions) and a Renilla luciferase control plasmid. After 48 hours, cell lysates were prepared, and luciferase activities were measured using the Dual-Luciferase Reporter Assay Kit. Firefly luciferase activity was normalized to Renilla activity, and relative luciferase activity was calculated as the ratio of firefly to Renilla luminescence.

Enzyme-linked immunosorbent assay (ELISA) for human FGF2

FGF2 secretion by Cal27 cells was measured

using the Human FGF2 ELISA Kit. Conditioned media or standards (100 μ L) were added to a pre-coated 96-well plate and incubated for 2 hours at 37°C. After washing, biotinylated detection antibody and HRP-streptavidin were added. Following substrate addition, absorbance at 450 nm was measured, and FGF2 concentrations were determined from a standard curve and expressed in pg/mL.

Preparation of conditioned medium

Conditioned medium for ELISA, Western blot, CCK-8, tube formation, and Matrigel plug assays was prepared by culturing Cal27 cells in serum-free DMEM for 24 hours after reaching 80% confluence. The medium was collected, centrifuged at 3,000 rpm for 20 minutes, and stored at -80°C for downstream analysis to assess its effects on HUVECs.

Transwell co-culture migration assays

Transwell co-culture migration assays were performed in 24-well plates with 8 μ m pore size. Cal27 cells were plated in the bottom chamber, and HUVECs (3×10^4 cells/well) were seeded in the upper chamber in serum-free ECM. After 20 hours of incubation at 37°C with 5% CO₂, migrated HUVECs were stained and photographed.

Tube formation assay

Matrigel was mixed with Cal27 supernatants in a 1:1 ratio and added to 96-well plates. After 30 minutes, HUVECs (2.5×10^4 cells/well) were seeded and incubated for 1-3 hours. For PD166866 treatment, Matrigel was mixed with DMEM, and HUVECs were treated with PD166866 for 24 hours before seeding in ECM. High-resolution images of the capillary-like structures were captured using an inverted light microscope. Quantitative analysis was performed using the Angiogenesis Analyzer plugin for ImageJ software (NIH). To comprehensively assess the angiogenic ability, the following four parameters were quantified: 1) Number of junctions: the number of branching points connecting segments, indicating the complexity of the vascular network; 2) Number of meshes: the number of enclosed polygonal areas, reflecting the maturity of tube formation; 3) Number of segments: the count of individual linear vessel elements delimited by junctions; 4) Total segments length: the sum of the lengths of all segments, representing the overall extension capability of the endothelial cells.

Matrigel plug assay

A Matrigel plug assay was performed to assess the effects of Cal27 supernatants on HUVECs. A mixture of 100 μ L Matrigel, 100 μ L Cal27

supernatants, and 1×10^6 HUVECs was implanted into nude mice. After two weeks, the mice were euthanized, and the Matrigel plugs were excised for analysis.

Hematoxylin and eosin (H&E), immunohistochemistry (IHC) and immunofluorescence (IF)

Tissue samples were fixed in 4% paraformaldehyde, dehydrated, cleared in xylene, and embedded in paraffin. Sections (5 μ m) were deparaffinized, rehydrated, and stained with hematoxylin and eosin (H&E) for light microscopy imaging. For IHC, sections underwent antigen retrieval, blocking, and incubation with primary and secondary antibodies. Immunoreactivity was detected using a DAB Substrate Kit, and nuclei were counterstained with hematoxylin. Staining intensity, area, and number were quantified using ImageJ software. For immunofluorescence (IF), sections followed the same antigen retrieval and blocking steps, incubated with primary antibodies, and then fluorophore-conjugated secondary antibodies. Nuclei were counterstained with DAPI, and images were captured using a digital slide scanner.

Multiple immunofluorescence (mIF)

For mIF, 5 μ m tissue sections were deparaffinized, rehydrated, and subjected to antigen retrieval in sodium citrate buffer. After blocking with 3% BSA, sections were incubated with primary antibodies (CD31, HMGA1, FGFBP1) overnight at 4°C, followed by secondary antibody incubation and fluorescein-conjugated tyramide signal amplification (TSA). Microwave treatment was applied to remove antibodies, and blocking was repeated. The last primary antibody (anti-FGF2) was incubated overnight, followed by Cy3-conjugated secondary antibody. Nuclei were stained with DAPI, and images were scanned using a digital slide scanner.

Masson's trichrome staining

Tissue sections were deparaffinized by baking at 65°C for 60 minutes, followed by immersion in xylene and rehydration through graded ethanol. Slides were mordanted with Bouin's solution, stained with Weigert's hematoxylin, and differentiated in acidic ethanol. Sections were stained with Biebrich scarlet-acid fuchsin, treated with phosphomolybdic acid, and stained with aniline blue. After dehydration, clearing in xylene, and mounting with neutral balsam, images were scanned using a digital slide scanner.

Tumor-bearing mouse model and PD166866 treatment

To establish a tumor-bearing mouse model, 8×10^5 Cal27 cells were injected subcutaneously into BALB/c nude mice. When tumors reached 20-30 mm³, mice were randomized into two groups: PD166866 treatment (30 mg/kg every two days for 30 days) or vehicle control (0.5% sodium carboxymethyl cellulose in saline).

Statistical analysis

Statistical analyses were performed using GraphPad Prism 9.0. Normality was assessed with the Shapiro-Wilk test, and variances were evaluated using the F test or Bartlett test. For two-group comparisons, a 2-tailed Student's unpaired t-test was used for normally distributed data with equal variances, Welch's correction for unequal variances, and the Mann-Whitney test for non-normally distributed data. For multiple groups, one-way ANOVA with Dunnett's multiple comparisons test was applied for normally distributed data, and the Kruskal-Wallis test for non-normally distributed data. Two-way ANOVA with Šidák's test was used for two-factor comparisons. Survival was analyzed by the log-rank test, and correlation was assessed using Pearson's correlation coefficients. A p-value < 0.05 was considered statistically significant. Data are presented as mean \pm SD or SEM.

Results

HMGA1 is highly expressed and is associated with poor prognosis in HNSCC patients

To assess HMGA1 expression across multiple cancers, we analyzed data from GEPIA, showing elevated HMGA1 in various cancer types compared to normal tissues (**Fig. S1A**). In HNSCC, single-cell RNA-seq data (GSE181919) identified nine major cell types, with epithelial cells showing notably higher HMGA1 expression (**Fig. 1A-C**). Using inferCNV, we distinguished malignant from non-malignant epithelial cells, finding HMGA1 significantly elevated in malignant cells (**Figs. S1B and 1D-F**). Consistent results from TCGA-HNSCC and GEO cohorts confirmed higher HMGA1 expression in HNSCC than adjacent normal tissues (**Figs. 1G and S1C-E**). Immunohistochemistry (IHC) of HNSCC tissues (n=29) and adjacent normal tissues (n=13) further validated this finding (**Fig. 1H and I**). Additionally, higher HMGA1 levels correlated with shorter overall survival (OS) in HNSCC patients (**Figs. 1J and S1F**), suggesting HMGA1's link to poor prognosis.

HMGA1 silencing disrupts oncogenic properties of HNSCC *in vitro* and *in vivo*

We found that HMGA1 expression is higher in HNSCC cell lines (Cal27, SCC25, HSC2 and SCC15) compared to normal human oral epithelial cells (HOEC) (Fig. S2A and B). To explore HMGA1 function, we selected two siHMGA1 sequences to reduce HMGA1 mRNA and protein levels (Fig. 2A and B). CCK8, colony formation, scratch, transwell and Matrigel assays revealed that HMGA1 silencing inhibits proliferation, clonogenicity, migration, and invasion in HNSCC cells, underscoring its role in these oncogenic behaviors (Figs. 2C-H and S2C-E). Next, we investigated the role of HMGA1 in tumorigenesis *in vivo*. We constructed a short hairpin RNA (shRNA) based on the sequence of siHMGA1 1 and successfully silenced HMGA1 in Cal27 by lentiviral delivery (Fig. 2I, J). Using ELDA assay [36], we found that HMGA1 deficiency reduced the number, volume, weight of tumors as well as tumor-initiating cells, confirming HMGA1's importance in tumorigenesis (Figs. 2K, L and S2F, G).

HMGA1 regulates carcinogenic transcriptional network and induces FGFBP1 expression

To further investigate the mechanism of HMGA1, a regulator at the transcriptional level, we performed RNA sequencing in Cal27 cells with or without HMGA1 silencing. Gene ontology (GO) enrichment analysis revealed an HMGA1 signature of genes involved in biological processes related to tumor progression, such as cell cycle and proliferation, cell migration and invasion, and especially, angiogenesis (Fig. 3A). Single sample gene set enrichment analysis (ssGSEA, MSigDb Hallmark gene sets) identified great diversity of the sample activity in 50 hallmark gene sets (Fig. 3B). Unexpectedly, angiogenesis pathway is also enriched (Fig. 3C, D). This suggests the potential effect of HMGA1 on angiogenesis in HNSCC. Differentially expressed genes (DEGs) (adjusted $P < 0.05$, $|\log_2(\text{siHMGA1}/\text{control})| \geq 0.5$) included 190 up- and 207 downregulated genes (Fig. 3E, listed in Supplemental Table 3).

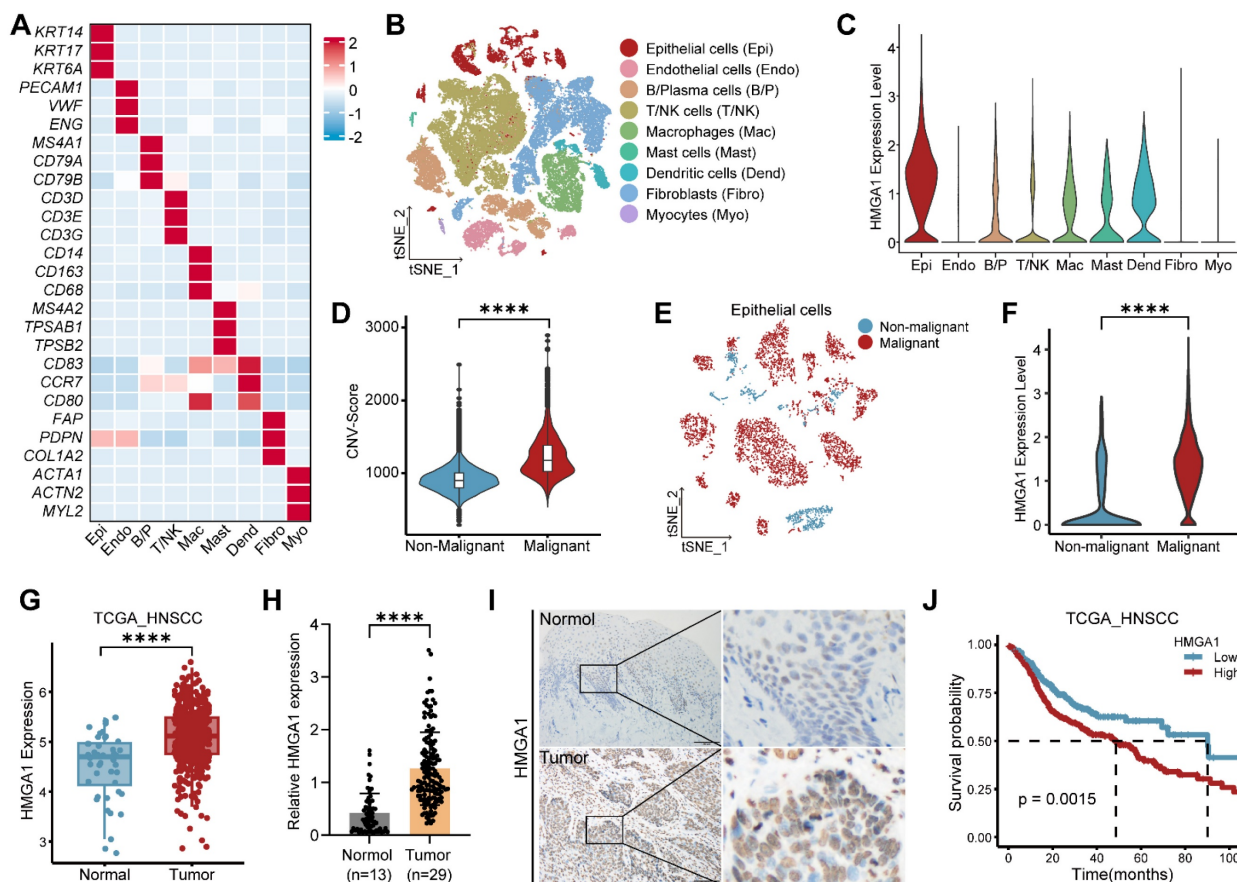


Figure 1. HMGA1 is highly expressed and is associated with poor prognosis in HNSCC. (A) Heatmap of signature genes for distinct cell types, which are represented by three specifically expressed genes. (B) The tSNE plot of the 53,232 cells delineates their cell types, with distinct colors distinguishing cell types. (C) Violin plot showing expression of HMGA1 in distinct cell types. (D) Violin plot showing CNV scores between non-malignant cells and malignant cells. (E) The tSNE plot showing the distribution of non-malignant epithelial cells (blue) and malignant epithelial cells (red). (F) Violin plot showing expression of HMGA1 between non-malignant epithelial cells (blue) and malignant epithelial cells (red). Data (A-F) are from scRNA-seq (GSE181919). (G) Boxplot showing expression of HMGA1 between normal (n=44 patients) and tumor (n=516 patients) in the TCGA-HNSCC cohort. (H, I) IHC showing the expression of HMGA1 in adjacent tissues (n=13 patients) and tumors (n=29 patients) with HNSCC. Scale bars: 100µm. (J) The Kaplan-Meier overall survival curves between low-HMGA1 group (n=177 patients) and high-HMGA1 group (n=339 patients) of TCGA-HNSCC cohort. Results are shown as mean ± standard deviation (SD). **** $P < 0.0001$; 2-tailed Student's unpaired t-test (D, F and G), Mann-Whitney test (H), log-rank test (J).

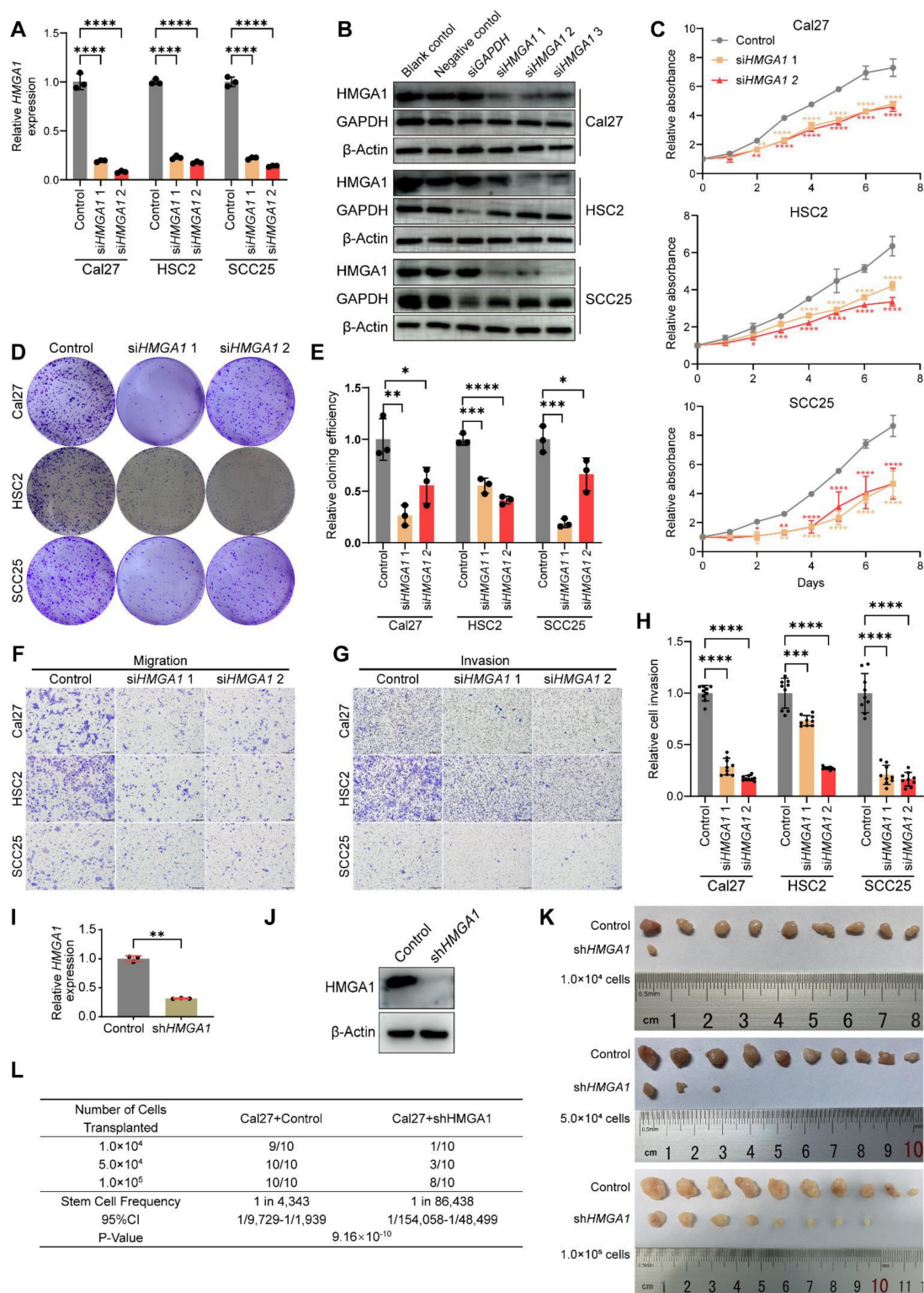


Figure 2. HMGAI silencing disrupts oncogenic properties of HNSCC in vitro and in vivo. (A) qRT-PCR showing the expression of HMGAI mRNA in HNSCC cell lines (Cal27, HSC2, SCC25) with and without HMGAI silencing via siRNA targeting 2 different sequences (siRNA1, siRNA2) from 3 experiments performed in triplicate. (B) Western blot (n = 3 independently biological experiments) showing the expression of HMGAI protein in HNSCC cells with and without HMGAI silencing. (C) CCK-8 assay showing the proliferation ability of HNSCC cells with and without HMGAI silencing from 3 experiments performed in triplicate. (D, E) Clonogenic assay showing the clonogenic ability of HNSCC with and without HMGAI silencing from 3 experiments performed in triplicate. (F) Transwell migration assay showing the migration ability of HNSCC cells with and without HMGAI silencing following treatment with 10μM cytosine β-D-arabinoside (Ara-C) for 1 hour to mitigate effects of proliferation from 3 experiments performed in triplicate. Scale bars: 200μm. (G, H) Matrigel invasion assay showing the invasive ability of HNSCC cells with and without HMGAI silencing following treatment with 10μM Ara-C for 1 hour from 3 experiments performed in triplicate. Scale bars: 200μm. (I, J) qRT-PCR and western blot (n = 3 independently biological experiments in I and J) showing the expression of HMGAI mRNA and protein in Cal27 cells with and without HMGAI silencing via lentiviral delivery of shRNA targeting the same sequence as siHMGA1 1. (K) In vivo limiting dilution assay showing xenograft tumorigenicity of Cal27 cells with and without HMGAI silencing at different limiting dilutions (n=10/condition). (L) Extreme limiting dilution analysis (ELDA) showing the frequency of tumor initiator cells. Data show 95% confidence interval around tumor initiator cell frequency (L). Results are shown as mean ± SD (A, C, E, H, I). *P<0.05, **P<0.01, ***P<0.001, ****P<0.0001; ordinary 1-way ANOVA with Dunnett's multiple comparisons test (A, C, E). Brown-Forsythe and Welch's ANOVA test with Dunnett's T3 multiple-comparisons test (H). 2-tailed Student's unpaired t-test with Welch's correction (I), chi-square test (L).

Interestingly, our data showed that the expression of fibroblast growth factor-binding protein 1 (*FGFBP1*) was reduced after silencing *HMGA1* (Fig. 3E), and *FGFBP1* is also involved in angiogenesis [37]. In addition, *HMGA1* and *FGFBP1* correlated positively (Fig. 3F-I). Single-cell RNA-seq data (GSE181919) showed that *FGFBP1* was most expressed in epithelial cells and was higher in malignant than nonmalignant epithelium (Fig. 3J, K). Consistent with this, *FGFBP1* expression was also higher in HNSCC cell lines than in HOEC (Fig. 3L). Therefore, we first focused on *FGFBP1*. We further found that silencing *HMGA1* reduced *FGFBP1* expression (mRNA, protein) (Fig. 3M, N). These results provide preliminary evidence for a link between *HMGA1* and *FGFBP1*.

Silencing *FGFBP1* recapitulates effects of silencing *HMGA1*

We further investigated the role of *FGFBP1* in HNSCC. First, we successfully silenced *FGFBP1* (mRNA and protein) in HNSCC cell lines (Fig. 4A, B). We found that *FGFBP1* deficiency recapitulated the inhibitory effect of *HMGA1* silencing on HNSCC. At the cellular level *in vitro*, *FGFBP1* deficiency inhibited proliferation, clonogenicity, migration, and invasion, consistent with the findings of Shintani et al [38] (Figs. 4C-H and S3A-C).

Using 5-ethynyl-2'-deoxyuridine (EdU) experiments, we demonstrated that silencing *HMGA1* or *FGFBP1* inhibited DNA synthesis in HNSCC cells, and overexpression of *FGFBP1* or addition of human FGF2 protein reversed this inhibition, suggesting that *FGFBP1* and FGF2 mediates the proliferative effect of *HMGA1* (Fig. S3D-G).

Next, we successfully constructed Cal27 cells with stable *FGFBP1* silencing by lentiviral delivery using shRNA (Fig. 4I, J). We used xenograft mice to investigate the effect of *FGFBP1* on tumorigenesis ability, and simultaneously performed ELDA analysis [36]. Like *HMGA1* silencing, *FGFBP1* deficiency inhibited tumorigenesis and reduced the proportion of tumor-initiating cells (Figs. 4K, L and S3H, I).

HMGA1 activates *FGFBP1* transcription by binding to its promoter

HMGA1 is a transcriptional regulator by binding to noncoding regions on DNA. To further explore the link between *HMGA1* and *FGFBP1*, first, we predict that *HMGA1* has a binding site on the promoter of *FGFBP1* by using the online website hTFtarget. This site is located from -936 to -922 base pairs upstream of the transcription start site (TSS) of *FGFBP1*, and we designated it R (Fig. 5A). First, we determined the optimal concentration (1U/100 μ L) of Micrococcal Nuclease (MNase) in HNSCC cells (Fig. 5B). A pair of

primers were designed for this site, and the length of the product was 142 bp. Next, we performed ChIP-qPCR and agarose gel electrophoresis and found that the proportion of DNA fragments containing this site in the silencing group was less than that in the control group, which was verified in all three HNSCC cells (Fig. 5C and D). Thus, we demonstrated that *HMGA1* can bind directly to the promoter of *FGFBP1*.

To investigate whether *HMGA1* transcriptionally activates *FGFBP1*, we further performed a dual luciferase reporter gene assay. The wild-type promoter of *FGFBP1* was constructed upstream of the luciferase gene. Compared with the control group, the luciferase expression in the silencing *HMGA1* group was lower, indicating that *HMGA1* transcriptionally activates *FGFBP1*. To investigate whether *HMGA1* binding site R is a functional site, we next mutated this site (5'-CCTGCATTTTCTCAG-3' to 5'-CCCGGGGCCCCGGGG-3'). The mutant promoter was constructed upstream of the luciferase gene. Compared with the wild type, the expression of luciferase in the mutant group was lower, indicating that this site is also a functional site. In addition, after silencing *HMGA1*, the luciferase expression was still decreased in the mutant group, indicating that there are other functional binding sites besides this site (Fig. 5E). These results were also demonstrated by overexpression of *HMGA1* (Fig. 5F-H).

In summary, we have identified a deep molecular biological connection between *HMGA1* and *FGFBP1*. *HMGA1* directly binds to the promoter of *FGFBP1* and transcriptionally activates it.

HMGA1 alters *FGFBP1*/*FGF2*/*FGFR1* and downstream signals

FGFBP1, a molecular chaperone of the fibroblast growth factor 2 (FGF2), increases the extracellular secretion of FGF2 [37,39]. FGF2 binds the fibroblast growth factor receptor 1 (FGFR1) to activate downstream signaling pathways, such as ERK/AKT [40]. Therefore, we hypothesized that *HMGA1* could increase the expression of *FGFBP1* to promote the secretion of FGF2 and further activate the downstream signaling pathway of FGFR1. To test this hypothesis, we found that silencing *HMGA1* or *FGFBP1* reduced the secretion of FGF2 in the supernatant (WB and ELISA), and overexpression of *FGFBP1* reversed this decrease (Fig. 5I-K). In addition, various downstream phosphorylated effector proteins were reduced after silencing *HMGA1* or *FGFBP1*, including p-FGFR1, p-ERK1/2, and p-AKT (Fig. 5J, K). Therefore, we can reasonably assume that *HMGA1* exerts its biological functions at least in part through *FGFBP1*/*FGF2*/*FGFR1* pathway.

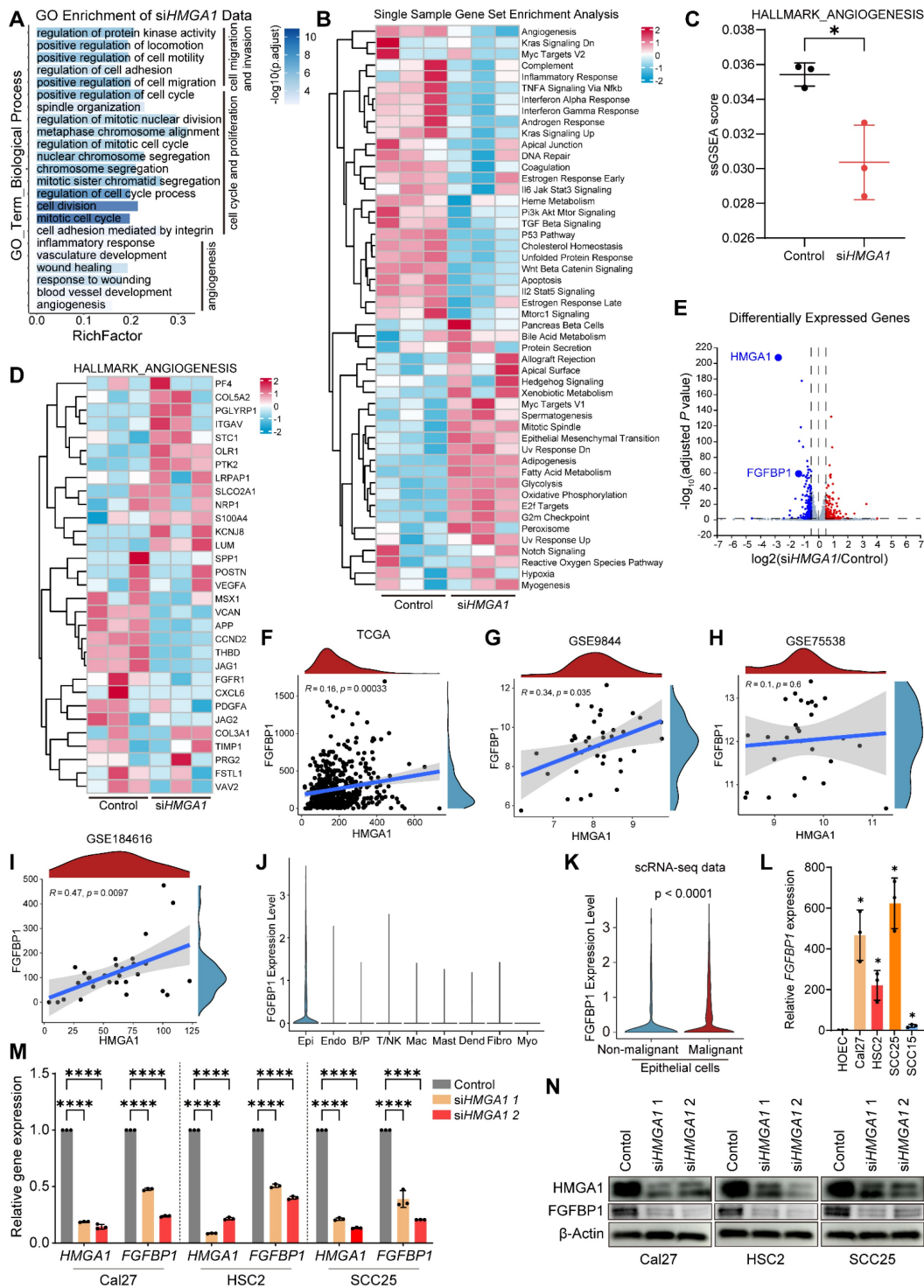


Figure 3. HMGAI regulates carcinogenic transcriptional network and induces FGFBP1 expression. (A) GO analysis of differentially expressed genes (DEGs) in RNA-seq data of Cal27 cells with and without *HMGAI* silencing. (B) Single sample gene set enrichment analysis (ssGSEA) showing the different enrichment of DEGs for different gene sets (MSigDb Hallmark) in Cal27 cells with and without *HMGAI* silencing. The colors are encoded by values of the ssGSEA scores in different samples. (C) ssGSEA showing the differential enrichment of DEGs for gene sets associated with angiogenesis (MSigDb Hallmark) in Cal27 cells with and without *HMGAI* silencing. (D) ssGSEA showing the different enrichment of genes in gene sets associated with angiogenesis (MSigDb Hallmark) in Cal27 cells with and without *HMGAI* silencing. (E) Volcano plot showing DEGs (1123 up- and 1375 downregulated) in Cal27 with and without *HMGAI* silencing. The genes most repressed with *HMGAI* silencing. Thresholds are shown as dashed lines. Adjusted $P < 0.05$, $|\log_2(\text{siHMGAI}/\text{control})| \geq 0.5$. (F) Correlation analysis of *HMGAI* and *FGFBP1* expression in TCGA-HNSCC cohort. 95% confidence interval (CI) is indicated with gray color. (G) Correlation analysis of *HMGAI* and *FGFBP1* expression in GSE9844 cohort. 95% confidence interval (CI) is indicated with gray color. (H) Correlation analysis of *HMGAI* and *FGFBP1* expression in GSE75538 cohort. 95% confidence interval (CI) is indicated with gray color. (I) Correlation analysis of *HMGAI* and *FGFBP1* expression in GSE184616 cohort. 95% confidence interval (CI) is indicated with gray color. (J) Violin plot showing expression of *FGFBP1* in distinct cell types. (K) Violin plot showing expression of *FGFBP1* between non-malignant epithelial cells (blue) and malignant epithelial cells (red). Data (J, K) are from scRNA-seq (GSE181919). (L) qRT-PCR showing the expression of *HMGAI* and *FGFBP1* mRNA in HNSCC cell lines (Cal27, HSC2, SCC25, SCC15) from 1 experiment performed in triplicate. (M) qRT-PCR showing the expression of *HMGAI* and *FGFBP1* mRNA in HNSCC cells (Cal27, HSC2, SCC25) with and without *HMGAI* silencing from 3 experiments performed in triplicate. (N) Western blot ($n = 3$ independently biological experiments) showing the expression of *HMGAI* and *FGFBP1* protein in HOEC and HNSCC cells with and without *HMGAI* silencing. Data shown as mean \pm SD. * $P < 0.05$, **** $P < 0.0001$; 2-tailed Student's unpaired t-test (C, K), 2-tailed Student's unpaired t-test with Welch's correction (L), ordinary 1-way ANOVA with Dunnett's multiple comparisons test (M).

HMGA1 enables HNSCC cells to induce HUVECs to form vessels via FGFBP1

Studies suggest HMGA1 and FGFBP1 promote angiogenesis, but their role in HNSCC remains unclear. We investigated this via several experiments. Our RNA-seq data indicated HMGA1-regulated genes are enriched in angiogenic pathways (Fig. 3A-D). FGFBP1 correlates with microvessel density in HNSCC tumors [41,42]. These suggest that HMGA1 and FGFBP1 may promote angiogenesis in HNSCC.

First, CCK8 assays revealed that supernatant from Cal27 cells with *HMGA1* or *FGFBP1* silencing reduced HUVECs' proliferation, while *FGFBP1* overexpression and added FGF2 (a pro-angiogenic factor) reversed this inhibition (Fig. 6A, B). Transwell co-cultures confirmed silencing *HMGA1* or *FGFBP1* inhibited Cal27-induced HUVECs' migration, which was reversed by *FGFBP1* overexpression or FGF2 (Fig. 6C-E). *In vitro* tube formation assays with Cal27-conditioned medium showed similar trends (Fig. 6F-H), which were quantitatively confirmed by analyzing four key parameters: the number of junctions, the number of meshes, the number of segments, and the total segments length (see the "Tube formation assay" section in Methods for details). We can reasonably speculate that silencing *HMGA1* or silencing *FGFBP1* reduces secretion of components that promote vascular endothelial proliferation and angiogenesis, while overexpression of *FGFBP1* released more FGF2 and reversed this reduction.

Next, a Matrigel plug assay in nude mice indicated that *HMGA1* or *FGFBP1* silencing produced lighter plugs, while *FGFBP1* overexpression or added FGF2 turned them redder (Fig. 6I, J). CD31 IHC showed lower CD31 in *HMGA1* or *FGFBP1* silencing groups, but higher levels with *FGFBP1* overexpression or added FGF2 (Fig. 6K-M). The above results were again confirmed by IF staining of typical Matrigel plugs with DAPI and CD31 (Fig. S4A). These results demonstrate that HMGA1 and FGFBP1 enable HNSCC cells to induce endothelial angiogenesis.

HMGA1 or FGFBP1 silencing reduces stromal formation, inhibits angiogenesis and causes tumor necrosis in HNSCC xenografts

IHC on xenograft tumors showed reduced CD31 levels in *HMGA1* or *FGFBP1* silencing groups, indicating decreased angiogenesis (Fig. 7A, B). IF results supported these findings (Fig. S4B). Additionally, Ki67-positive cells decreased, reflecting reduced proliferation, while *HMGA1* silencing lowered *FGFBP1* expression (Fig. 7A, B). Some

regions in the *shHMGA1* group still showed high HMGA1 levels, suggesting silencing escape may be necessary for tumor formation, aligning with previous studies [19].

Multiple immunofluorescence (mIF) staining (Fig. 7C) revealed decreased HMGA1 and FGFBP1 fluorescence in the *shHMGA1* group. Nuclear FGF2 was higher in the *shHMGA1* group, with a negative correlation between FGFBP1 and FGF2 fluorescence (Fig. 7C, solid lines and arrows), indicating reduced FGFBP1 leads to nuclear retention and decreased secretion of FGF2, consistent with Frank et al. [37]. Persistent high FGFBP1 expression in some regions suggests escape from *HMGA1* silencing. CD31 levels were lower, reflecting reduced angiogenesis.

More cell-free areas were observed in the *shHMGA1* group than in the control (Fig. 7C, dashed circles and arrows), suggesting increased tumor necrosis due to *HMGA1* silencing. H&E staining confirmed these necrotic areas, which lacked normal cellular structure and nearby blood vessel formation (Fig. 7D, dashed circles and arrows). No blood vessels were observed near two large cell-free regions in the *shHMGA1* group (Fig. 7C, the solid circle). This indicates that *HMGA1* silencing inhibits angiogenesis, leading to tumor necrosis. Similarly, *shFGFBP1* tumors showed more necrotic areas compared to controls (Fig. 7D, dashed circles and arrows), supporting that *FGFBP1* silencing also reduces angiogenesis and causes necrosis.

mIF results indicate reduced tumor stroma in the *shHMGA1* group compared to the control (Fig. 7C), confirmed by Masson trichrome staining (Fig. 7E, dashed circles), consistent with Lionel et al. [19]. Stroma was absent near necrotic areas in the *shHMGA1* group (Fig. 7E, dashed circles), while blood vessels formed in the control stroma (Fig. 7E, red arrows). As tumor stroma supports angiogenesis, *HMGA1* silencing likely reduces stroma and blood vessel formation, leading to necrosis and inhibited tumor growth.

HMGA1 and FGFBP1 together predict the prognosis of HNSCC patients

Pan-cancer analysis (GEPIA) showed *FGFBP1* expression varied across tumors (Fig. S4A). RNA-seq data (TCGA-HNSCC, GEO) revealed no significant differences between HNSCC and controls (Fig. S5B-E). Begum et al. and Li et al. reported high *FGFBP1* expression in HNSCC [41,42], while Bem et al. found the opposite [43]. IHC showed lower *FGFBP1* expression in tumors compared to adjacent margins (Fig. S5F, G). *FGFBP1* expression varied within tumors, suggesting its potential prognostic role. Then, we found higher *FGFBP1* levels correlated

with shorter overall survival (OS) in HNSCC patients (Fig. S5H). We divided patients into four subgroups based on HMGA1 and FGFBP1 expression. Notably, high FGFBP1 expression predicted worse prognosis in

the HMGA1 low group, while low FGFBP1 expression predicted worse outcomes in the HMGA1 high group, aiding HNSCC prognosis assessment (Fig. S5J).

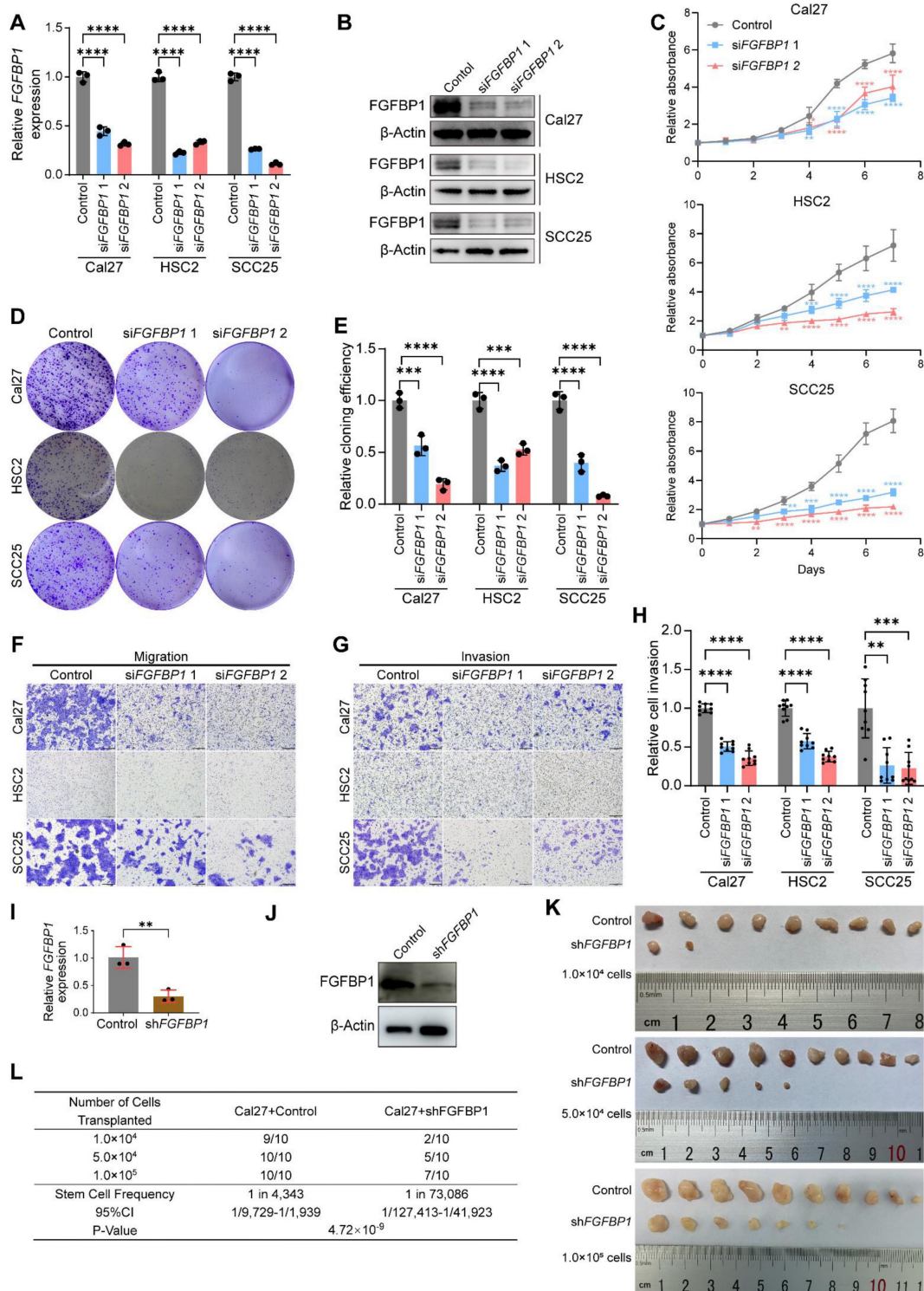


Figure 4. *FGFBP1* silencing recapitulates effects of *HMGA1* silencing in HNSCC *in vitro* and *in vivo*. (A) qRT-PCR showing the expression of *FGFBP1* mRNA in HNSCC cell lines (Cal27, HSC2, SCC25) with and without *FGFBP1* silencing via siRNA targeting 2 different sequences (siRNA1, siRNA2) from 3 experiments performed in triplicate. (B) Western blot ($n = 3$ independently biological experiments) showing the expression of *FGFBP1* protein in HNSCC cells with and without *FGFBP1* silencing. (C) CCK-8 assay showing the proliferation ability of HNSCC cells with and without *FGFBP1* silencing from 3 experiments performed in triplicate. (D, E) Clonogenic assay showing the clonogenic ability of HNSCC with and without *FGFBP1* silencing from 3 experiments performed in triplicate. (F) Transwell migration assay showing the migration ability of HNSCC cells with and without *FGFBP1* silencing following treatment with 10 μ M cytosine β -D-araboside (Ara-C) for 1 hour to mitigate effects of proliferation from 3

experiments performed in triplicate. Scale bars: 200µm. **(G, H)** Matrigel invasion assay showing the invasive ability of HNSCC cells with and without *FGFBP1* silencing following treatment with 10µM Ara-C for 1 hour from 3 experiments performed in triplicate. Scale bars: 200µm. **(I, J)** qRT-PCR and western blot ($n = 3$ independently biological experiments in **I** and **J**) showing the expression of *FGFBP1* mRNA and protein in Cal27 cells with and without *FGFBP1* silencing via lentiviral delivery of shRNA targeting the same sequence as si*FGFBP1* 2. **(K)** *In vivo* limiting dilution assay showing xenograft tumorigenicity of Cal27 cells with and without *FGFBP1* silencing at different limiting dilutions ($n=10$ /condition). **(L)** ELDA showing the frequency of tumor initiator cells. Data show 95% confidence interval around tumor initiator cell frequency **(L)**. Data shown as mean \pm SD **(A, C, E, H, I)**. * $P < 0.05$, ** $P < 0.01$, *** $P < 0.001$, **** $P < 0.0001$; ordinary 1-way ANOVA with Dunnett's multiple comparisons test **(A, C, E, Cal27 and HSC2 of H)**, Kruskal-Wallis test with Dunn's multiple-comparison test **(SCC25 of H)**, 2-tailed Student's unpaired t-test **(I)**, chi-square test **(L)**.

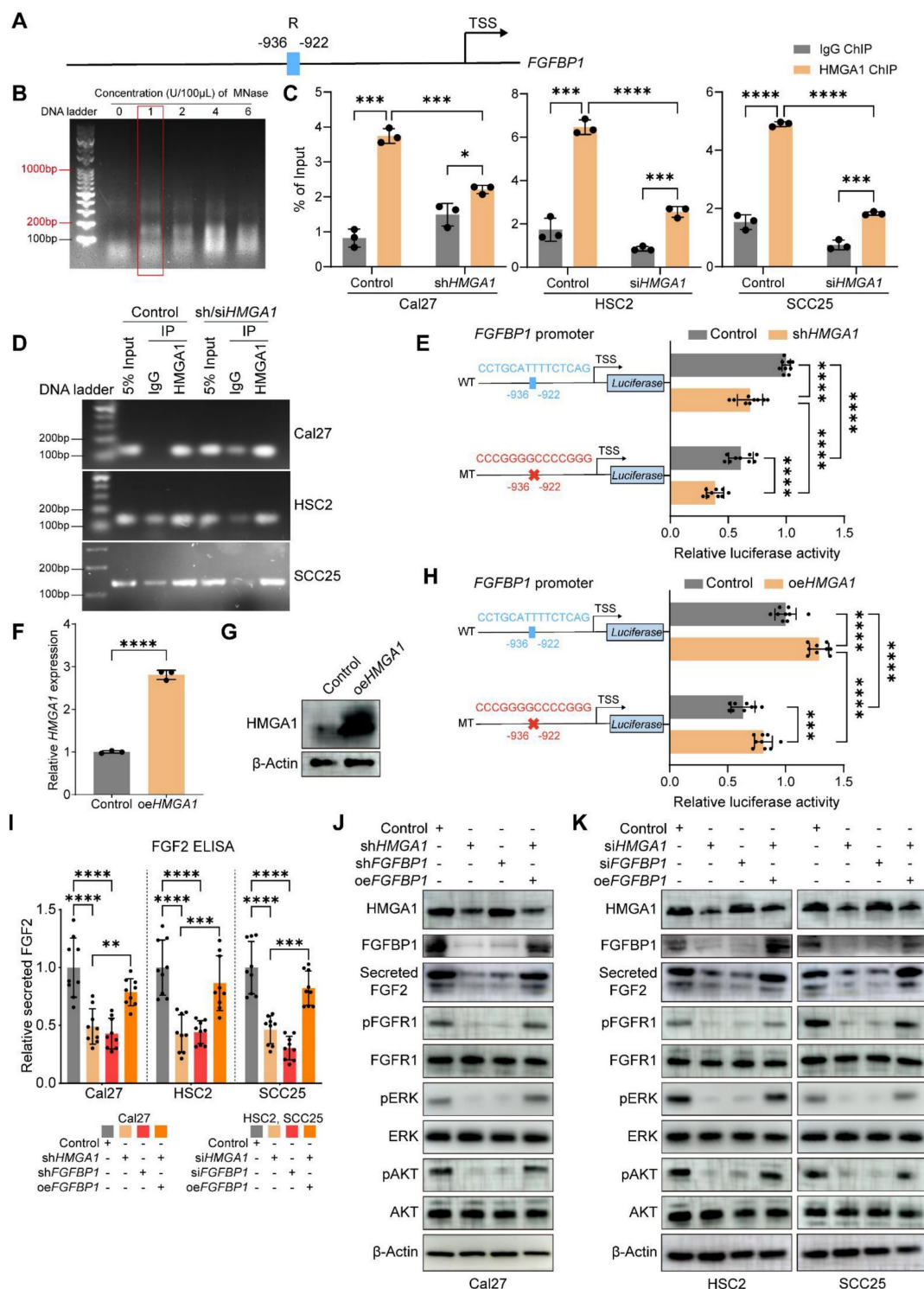


Figure 5. HMGAI activates *FGFBP1* transcription by binding to its promoter and alters *FGFBP1/FGF2/FGFR1* pathways. **(A) Schematic representation of the *FGFBP1* promoter; R is the predicted HMGAI binding site. **(B)** The extracted genomic DNA is sheared into smaller, workable pieces enzymatically by digestion with different concentrations of micrococcal nuclease (MNase). 1U/100µL is the optimal concentration which yields more fragments from 200 to 1000 base pairs. **(C, D)** ChIP-qPCR and agarose gel electrophoresis showing HMGAI occupancy on the *FGFBP1* promoter in HNSCC cells (Cal27, HSC2, SCC25) with and without *HMGAI* silencing. **(E)** Dual-luciferase reporter gene assay showing the transcriptional activation ability of HMGAI on *FGFBP1* promoter in Cal27 cells transfected with *HMGAI* silencing or control vector and *FGFBP1* promoter constructs including wild type and mutant type. The potential HMGAI binding site (-936/-922) is mutated from CCTGCATTTTCTCAG to CCCGGGGCCCCGGG. **(F, G)** qRT-PCR and western blot ($n = 3$ independently biological experiments in **F** and **G**) showing the expression of HMGAI mRNA and protein in Cal27 cells with and without**

HMGA1 overexpression via plasmid delivery. **(H)** Dual-luciferase reporter gene assay showing the transcriptional activation ability of HMGA1 on *FGFBP1* promoter in Cal27 cells transfected with *HMGA1* overexpression or control vector and *FGFBP1* promoter constructs. **(I)** ELISA showing the expression of secreted FGF2 in HNSCC cells under different conditions from 3 experiments performed in triplicate. **(J, K)** Western blot ($n = 3$ independently biological experiments) showing the expression of secreted FGF2, FGFR1 and its downstream signaling molecules (ERK, AKT), including total and phosphorylated proteins in HNSCC cells under different conditions (control, *HMGA1* silencing, *FGFBP1* silencing, *HMGA1* silencing + *FGFBP1* overexpressing). shRNA is used to silence *HMGA1* and *FGFBP1* in Cal27, while siRNA is used in HSC2 and SCC25. Data shown as mean \pm SD. *** $P < 0.001$, **** $P < 0.0001$; 2-tailed Student's unpaired *t*-test **(C, MT (shHMGA1 control), shHMGA1 (WT MT), F, H)**, 2-tailed Student's unpaired *t*-test with Welch's correction **(WT(shHMGA1 control) and Control(WT MT))**, ordinary 1-way ANOVA with Dunnett's multiple comparisons test **(I)**.

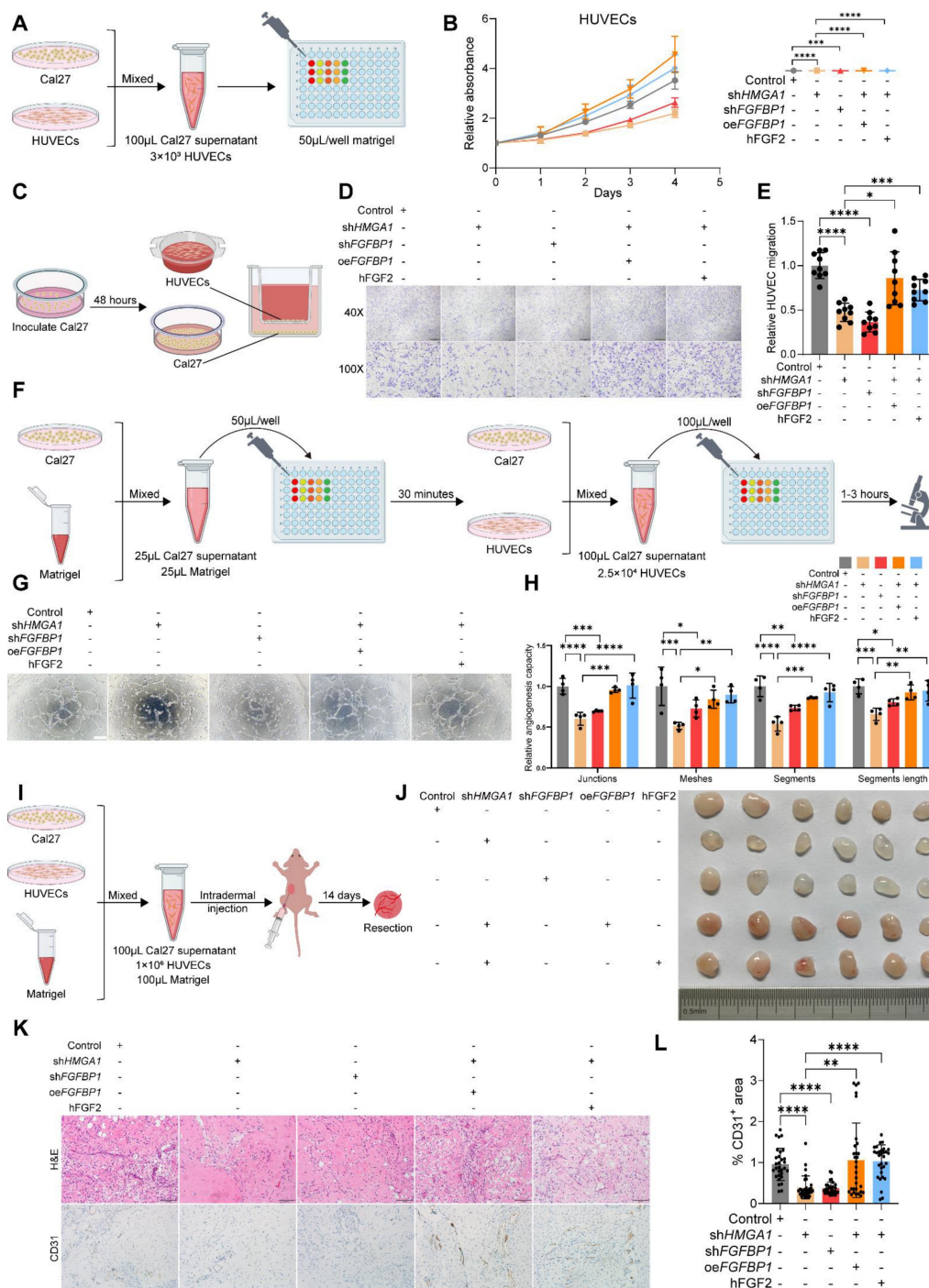


Figure 6. HMGA1 enables HNSCC cells to induce HUVECs to form vessels via FGFBP1. **(A, B)** CCK-8 showing the proliferation ability of HUVECs treated with different conditioned supernatants of Cal27 cells (control, *HMGA1* silencing, *FGFBP1* silencing, *HMGA1* silencing + *FGFBP1* overexpressing, *HMGA1* silencing + 100ng/mL hFGF2) from 3 experiments performed in triplicate. **(C-E)** Transwell co-culture assay showing the migration ability of HUVECs co-cultured with Cal27 cells under different conditions from 3 experiments performed in triplicate. Scale bar, $\times 40$ magnification, 500 μm ; scale bar, $\times 100$ magnification, 200 μm . **(F-H)** Tube formation assay ($n = 4$ per condition) showing the *in vitro* angiogenic ability of HUVECs treated with different conditioned supernatants of Cal27 cells (control, *HMGA1* silencing, *FGFBP1* silencing, *HMGA1* silencing + *FGFBP1* overexpressing, *HMGA1* silencing + 100ng/mL hFGF2). **(I, J)** Matrigel plug assay ($n = 6$ per condition) showing the *in vivo* angiogenic ability of HUVECs treated with different conditioned supernatants of Cal27 cells (control, *HMGA1* silencing, *FGFBP1* silencing, *HMGA1* silencing + *FGFBP1* overexpressing, *HMGA1* silencing + 100ng/mL hFGF2). **(K, L)** % CD31⁺ area of the IHC for CD31 and cell nucleus of the Matrigel plug showing the *in vivo* angiogenic ability of HUVECs treated with different conditioned supernatants of Cal27 cells (control, *HMGA1* silencing, *FGFBP1* silencing, *HMGA1* silencing + *FGFBP1* overexpressing, *HMGA1* silencing + 100ng/mL hFGF2). Scale bar, 100 μm . Data from 5 fields at $\times 20$ magnification of tumors from 6 different mice per condition. Data shown as mean \pm SD. * $P < 0.05$, ** $P < 0.01$, *** $P < 0.001$, **** $P < 0.0001$; 2-way ANOVA with Šidák's multiple comparisons test **(B)**, Brown-Forsythe and Welch's ANOVA test with Dunnett's T3 multiple-comparisons test **(E)**, ordinary 1-way ANOVA with Dunnett's multiple comparisons test **(H)**, Kruskal-Wallis test with Dunn's multiple-comparison test **(L)**.

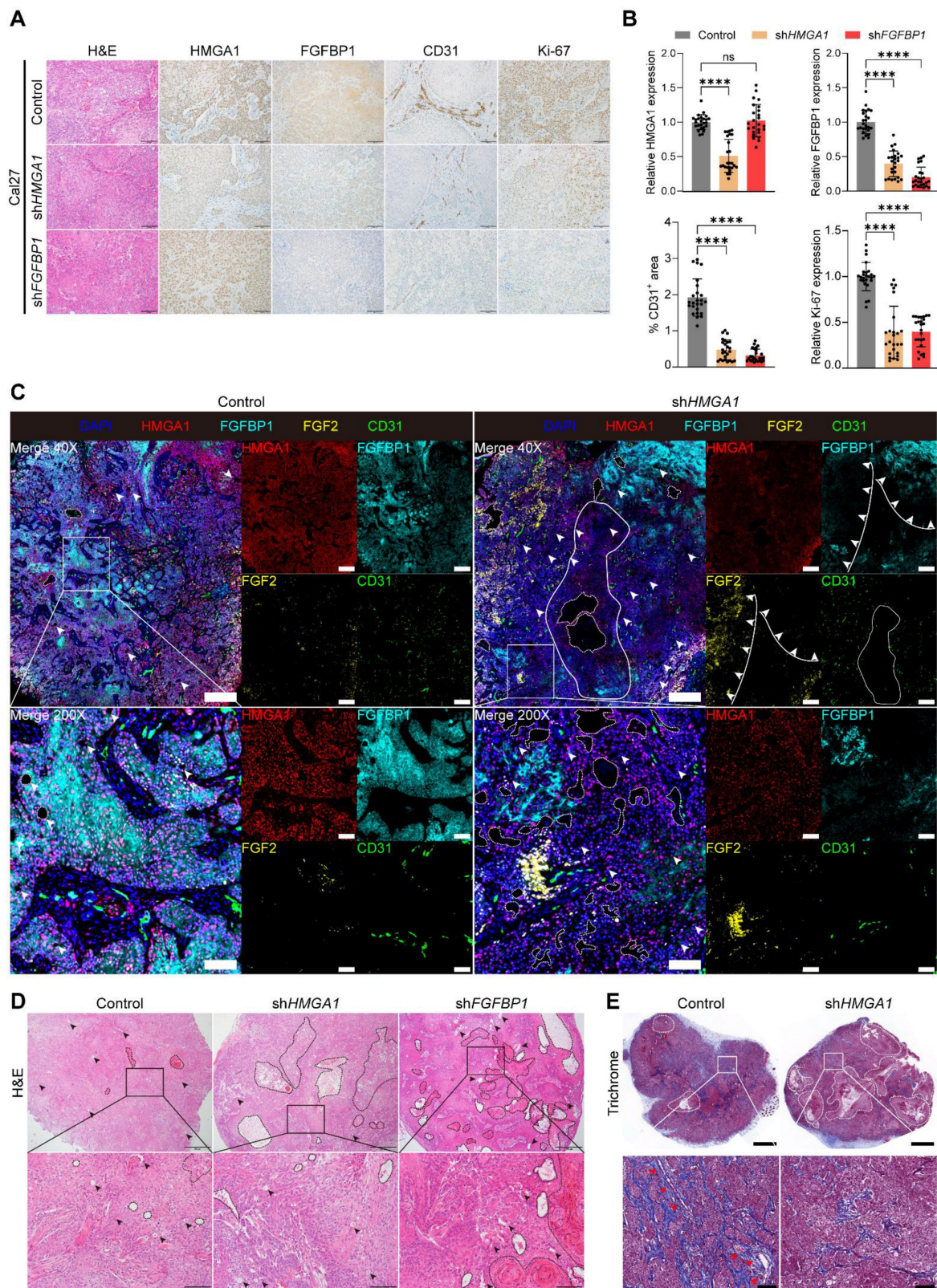


Figure 7. HMGAI or FGFBP1 silencing reduces stromal formation, inhibits angiogenesis and causes tumor necrosis in HNSCC xenografts. (A, B) H&E staining and IHC for HMGAI, FGFBP1, CD31, Ki67 in Cal27 xenografts with and without HMGAI or FGFBP1 silencing. Data from 5 fields at ×200 magnification of tumors from 5 different mice per condition. Scale bar, 100 μm. **(C)** Representative images of mIF for HMGAI, FGFBP1, FGF2, CD31 in Cal27 xenografts with and without HMGAI or FGFBP1 silencing. Dashed circles and arrows: cell-free regions; solid circle: avascular region; solid lines plus arrows: regions with low or high expression of FGFBP1 and FGF2. Scale bar, 500 μm; scale bar, local magnification, 100μm. **(D)** Representative images of H&E staining in Cal27 xenografts with and without HMGAI or FGFBP1 silencing. Dashed circles and arrows: cell-free and necrotic regions. Scale bar, 500 μm; scale bar, local magnification, 100μm. **(E)** Representative images of Masson's trichrome staining in Cal27 xenografts with and without HMGAI silencing. Dashed circles: stroma-free and cell-free regions; red arrows: vessels. Scale bar, 1 mm; scale bar, local magnification, 100μm. Control group and shHMGAI group in **(C, D and E)** were from the same tumor, respectively. Data shown as mean ± SD. ns, not significant; ****P<0.0001; Kruskal-Wallis test with Dunn's multiple-comparison test **(B)**.

FGFR1 inhibitor PD166866 inhibits carcinogenesis and angiogenesis *in vivo* and *in vitro*

To improve clinical applicability, we tested PD166866, a FGFR1 inhibitor [44–46], on HNSCC. PD166866 inhibited proliferation, clonogenicity, migration, invasion of HNSCC cells, and tube formation of HUVECs (**Figs. 8A-F and S6A-E**). In nude mice, PD166866 reduced tumor size and weight, with two tumors disappearing entirely (**Fig. 8G-I**). IHC and IF showed lower CD31 and Ki67 levels, indicating reduced angiogenesis and proliferation (**Figs. 8J, M, N and S6F**). PD166866 also decreased HMGA1 and FGFBP1 expression and increased necrosis in xenografts (**Fig. 8J-L, O**).

Discussion

Epigenetic changes, which alter gene expression and contribute to malignant transformation, are key features of tumors [15]. Understanding these changes is crucial for improving cancer prevention and treatment. HMGA1, a chromatin regulator, is overexpressed in many cancers and plays a significant role in altering chromatin structure to promote malignancy [19–25]. However, its function in head and neck squamous cell carcinoma (HNSCC) remains poorly understood [26–28]. This study aims to explore the role of HMGA1 in HNSCC.

As a solid tumor, a troublesome feature of HNSCC is its internal blood vessels [47]. Our results show that silencing *HMGA1* and its target *FGFBP1* inhibits angiogenesis, leads to tumor necrosis, and suppresses tumor progression. Additionally, silencing *HMGA1* reduces tumor stroma formation, aligning with previous studies [19]. Single-cell sequencing revealed that HMGA1 is more highly expressed in malignant epithelial cells than in normal ones, indicating its role in carcinogenesis. Consistent with this, data from TCGA, GEO databases, and patient samples indicate that HMGA1 is overexpressed in HNSCC and correlates with poor prognosis. HMGA1 is known to maintain stemness in cells, and our study shows that silencing HMGA1 decreases tumor stem cells, which play a pivotal role in tumor development [48].

HMGA1 regulates gene expression, and transcriptome sequencing of HNSCC cells with and without HMGA1 silencing identified several biological processes linked to tumor progression, such as cell proliferation, migration, and angiogenesis. Notably, HMGA1 directly activates the transcription of *FGFBP1*, which, in turn, enhances the secretion of FGF2, a key factor in angiogenesis. Silencing *FGFBP1* replicated the effects of silencing HMGA1 in both

in vitro and *in vivo* experiments. Overexpression of *FGFBP1* or *FGF2* reversed the suppression of cell proliferation caused by HMGA1 silencing, suggesting that HMGA1 promotes tumorigenesis by upregulating *FGFBP1* in HNSCC.

Further analysis showed that HMGA1-regulated genes are enriched in angiogenesis-related pathways, and previous studies have shown that HMGA1 promotes angiogenesis [25,34]. In addition, *FGFBP1* is the molecular chaperone of FGF2, which promotes angiogenesis by releasing FGF2, a pro-angiogenic factor. We then confirmed that HMGA1 promotes angiogenesis in HNSCC through *FGFBP1* and FGF2. Silencing HMGA1 or *FGFBP1* reduced FGF2 secretion and hindered angiogenesis *in vitro* and *in vivo*. Overexpression of *FGFBP1* or FGF2 reversed these effects. In tumor-bearing mice, silencing HMGA1 or *FGFBP1* decreased blood vessels, explaining the inhibition of tumor growth. Additionally, tumor necrosis and reduced tumor stroma formation were observed, which is consistent with the idea that silencing HMGA1 impedes angiogenesis and tumor progression.

FGFR1 inhibitor PD166866, which blocks FGF2 signaling, mimicked the effects of HMGA1 or *FGFBP1* silencing, further supporting the role of the HMGA1-*FGFBP1*-FGF2 axis in tumor progression and angiogenesis. In HNSCC, previous studies and IHC results of our patients showed conflicting *FGFBP1* expression levels [41–43]. In patients with low HMGA1 expression, high *FGFBP1* expression predicts a poor prognosis, and in patients with high HMGA1 expression, low *FGFBP1* expression predicts a worse prognosis. This suggests that the co-survival analysis of HMGA1 and *FGFBP1* can refine prognosis prediction for HNSCC patients.

Notably, although our functional experiments clearly demonstrate the direct transcriptional activation of *FGFBP1* by HMGA1, their mRNA or protein levels did not show a completely consistent positive correlation in public databases or in our own clinical samples. This discrepancy may be due to the high heterogeneity of tumors, complex post-transcriptional regulation of *FGFBP1*, and cross-interference from other signaling pathways in the tumor microenvironment. Interestingly, the combined expression pattern of HMGA1 and *FGFBP1*, rather than the level of either molecule alone, exhibited stronger prognostic predictive power, suggesting that the functional relationship between the two may vary dynamically depending on the molecular context of the tumor. This further emphasizes the need to place the HMGA1-*FGFBP1* axis within the broader context of the tumor ecosystem in future translational research.

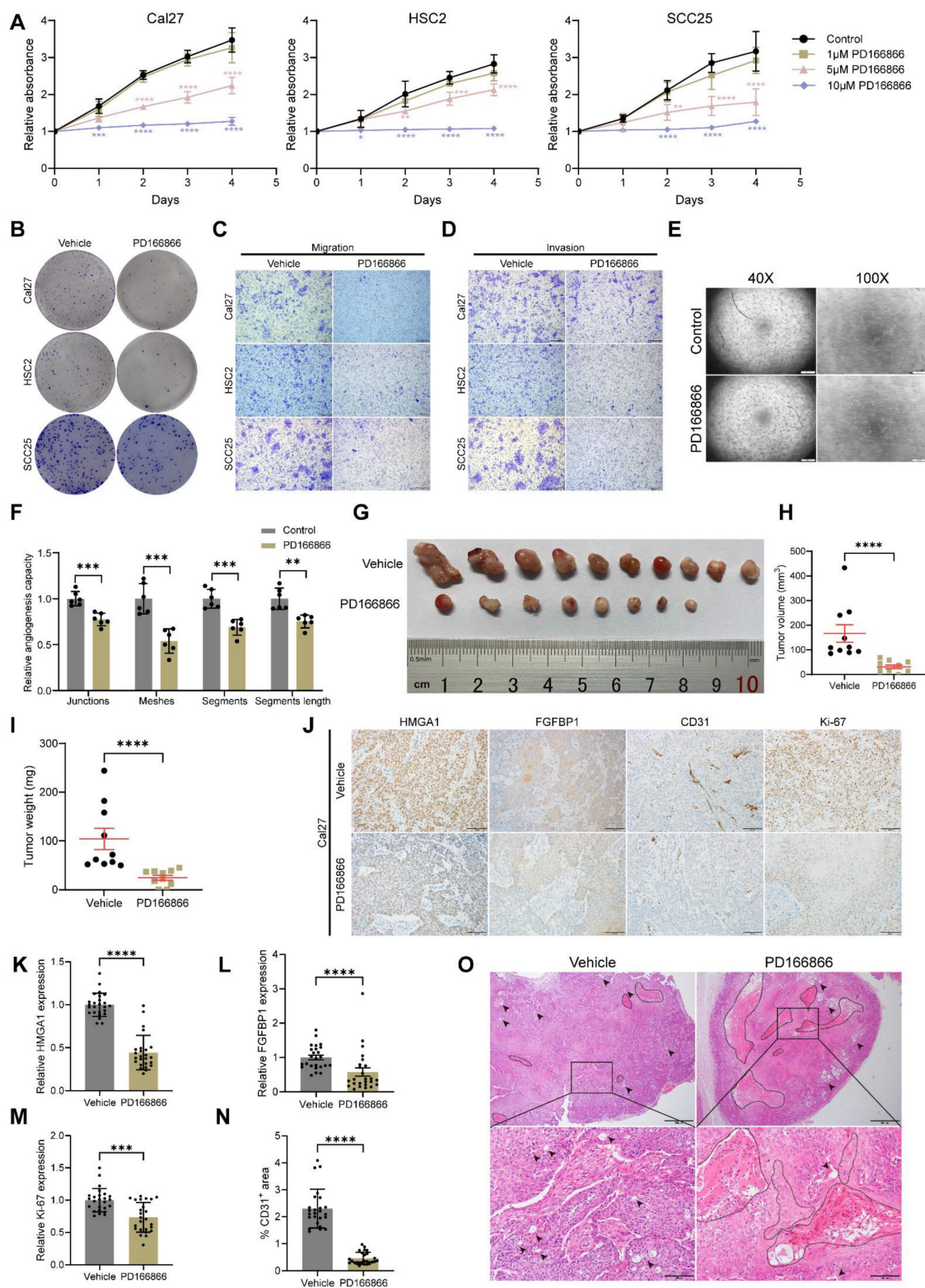


Figure 8. PD166866 inhibits carcinogenesis and angiogenesis in vivo and in vitro. (A) CCK-8 assay showing the proliferation ability of HNSCC cells with and without PD166866 treatment from 3 experiments performed in triplicate. (B) Clonogenic assay showing the clonogenic ability of HNSCC with and without PD166866 treatment from 3 experiments performed in triplicate. (C) Transwell migration assay showing the migration ability of HNSCC cells with and without PD166866 treatment following treatment with 10 μ M cytosine β -D-arabinoiside (Ara-C) for 1 hour to mitigate effects of proliferation from 3 experiments performed in triplicate. Scale bars: 200 μ m. (D) Matrigel invasion assay showing the invasive ability of HNSCC cells with and without PD166866 treatment following treatment with 10 μ M Ara-C for 1 hour from 3 experiments performed in triplicate. Scale bars: 200 μ m. (E, F) Tube formation assay showing the *in vitro* angiogenic ability of HUVECs with and without PD166866 treatment from 2 experiments performed in triplicate. Scale bar, \times 40 magnification, 500 μ m; scale bar, \times 100 magnification, 200 μ m. (G-I) Tumor number, volume, and weight comparisons from subcutaneous implantation of Cal27 cells in mice treated with PD166866 or vehicle control (n=10/condition). (J-N) IHC for HMGAI, FGFBP1, CD31, Ki67 in Cal27 xenografts with PD166866 or vehicle control. Data from 5 fields at \times 200 magnification of tumors from 5 different mice per condition. Scale bar, 100 μ m. (O) Representative images of H&E staining in Cal27 xenografts with PD166866 or vehicle control. Dashed circles and arrows: cell-free and necrotic regions. Scale bar, 500 μ m; scale bar, local magnification, 100 μ m. Data shown as mean \pm SD. * P <0.05, ** P <0.01, *** P <0.001, **** P <0.0001; ordinary 1-way ANOVA with Dunnett's multiple comparisons test (A), 2-tailed Student's unpaired *t*-test (F), Mann-Whitney test (H, I, K, M, N), 2-tailed Student's unpaired *t*-test with Welch's correction(L).

IHC analysis revealed that FGFBP1 was predominantly expressed in the basal side of tumor tissues, known as the progressive frontier or tumor budding, which is associated with more malignant cells [49,50]. Shahana et al. showed that the expression of FGFBP1, FGF2, and VEGFA became higher with the severity of oral epithelial dysplasia [41]. We also observed higher expression of HMGA1 at this site, suggesting that HMGA1 and FGFBP1 may play a crucial role in the later stages of tumor progression. This warrants further investigation.

Anti-angiogenic therapy in HNSCC faces challenges, including low treatment efficacy and high recurrence rates [51,52]. Growth factors are promising therapeutic targets, with antibodies or receptor inhibitors used to block their functions. Our study highlights the critical roles of HMGA1 and FGFBP1 in tumorigenesis and angiogenesis in HNSCC, offering new targets for anti-vascular therapy. We showed that HMGA1 upregulates FGFBP1, promoting FGF2 release, activating FGFR1, and triggering downstream pathways. This underscores the importance of the HMGA1-FGFBP1-FGF2-FGFR1 axis in HNSCC progression. Additionally, we demonstrated that targeting HMGA1 and FGFBP1 may provide a new therapeutic approach for HNSCC.

Abbreviations

Ara-C: cytosine β -D-arabinofuranoside; CCK8: cell counting kit-8; CHIP: chromatin immunoprecipitation; DEGs: differentially expressed genes; EdU: 5-ethynyl-2'-deoxyuridine; ELDA: extreme limiting dilution analysis; ELISA: enzyme-linked immunosorbent assay; FGFBP1: fibroblast growth factor-binding protein 1; FGFR1: FGF receptor 1; GO: gene ontology; H&E: hematoxylin and eosin; HMGA1: high mobility group AT-hook 1; HNSCC: head and neck squamous cell carcinoma; HOEC: human oral epithelial cells; HUVECs: human umbilical vein endothelial cells; IF: immunofluorescence; IHC: immunohistochemistry; mIF: multiple immunofluorescence; MNase: micrococcal Nuclease; OS: overall survival time; RNAseq: RNA sequencing; RT-qPCR: reverse transcriptase quantitative PCR; scRNA-seq: single-cell RNA-seq; shRNA: short hairpin RNA; ssGSEA: single sample gene set enrichment analysis; TSA: tyramide signal amplification; TSS: transcription start site; VEGF: vascular endothelial growth factor; WB: western blot.

Supplementary Material

Supplementary methods, figures and tables.
<https://www.ijbs.com/v22p3013s1.pdf>

Acknowledgements

Funding

This work was supported by Natural Science Foundation of Shandong Province (ZR2020QH157, ZR2021MH270, ZR2024MH115), Open foundation of Shandong Key laboratory of Oral Tissue Regeneration (SDDX202105), and National Natural Science Foundation of China (82470425).

Ethics approval and consent to participate

The use of HNSCC patient tissues was approved by the Ethics Committee of Shandong Provincial Hospital of Stomatology (Approval No. 20240403), with informed consent waived. Animal experiments were approved by the Animal Care and Use Ethics Committee of Shandong Provincial Hospital (Approval No. 2024-076). All experiments followed the approved protocols and guidelines, with tumor size not exceeding the 1500 mm³ limit.

Data availability statement

The processed single-cell transcriptome data and bulk transcriptome data used in this study obtained from: Choi (GSE181919, scRNA-seq), Zhou (GSE9844, RNA-seq), Mes (GSE85446, RNA-seq), Krishnan (GSE75538, RNA-seq), Satgunaseelan (GSE184616, RNA-seq), and TCGA-HNSCC (RNA-Seq). The RNA-seq data of this study are available in the NCBI Sequence Read Archive (SRA) with the accession numbers PRJNA1178083. Data and materials included in this article are provided in the Supplementary information. Any other information is also available upon request from the authors.

Author contributions

ZZ designed research studies, conducted experiments, acquired data, analyzed data and wrote the manuscript and also developed the bioinformatics analysis plan. YL X performed the bioinformatics analyses. MY L designed research studies, analyzed data and reviewed the manuscript. SY W conducted experiments. GD W, ZX L, XJ Y and HQ Z reviewed the manuscript. GL L and DS Z reviewed the manuscript. HW W designed research studies and contributed the funding. SY H designed research studies, contributed the funding and reviewed the manuscript.

Competing Interests

The authors have declared that no competing interest exists.

References

- Sung H, Ferlay J, Siegel RL, et al. Global Cancer Statistics 2020: GLOBOCAN Estimates of Incidence and Mortality Worldwide for 36 Cancers in 185 Countries. *CA Cancer J Clin.* 2021; 71: 209–49.
- Johnson DE, Burtneis B, Leemans CR, Lui VWY, Bauman JE, Grandis JR. Head and neck squamous cell carcinoma. *Nat Rev Dis Primers.* 2020; 6: 92.
- Bhat AA, Yousuf P, Wani NA, et al. Tumor microenvironment: an evil nexus promoting aggressive head and neck squamous cell carcinoma and avenue for targeted therapy. *Signal Transduct Target Ther.* 2021; 6: 12.
- Liu Z-L, Chen H-H, Zheng L-L, Sun L-P, Shi L. Angiogenic signaling pathways and anti-angiogenic therapy for cancer. *Signal Transduct Target Ther.* 2023; 8: 198.
- Argiris A, Li S, Savvides P, et al. Phase III Randomized Trial of Chemotherapy With or Without Bevacizumab in Patients With Recurrent or Metastatic Head and Neck Cancer. *J Clin Oncol.* 2019; 37: 3266–74.
- Adkins D, Ley JC, Liu J, Oppelt P. Ramucirumab in combination with pembrolizumab for recurrent or metastatic head and neck squamous cell carcinoma: a single-centre, phase 1/2 trial. *Lancet Oncol.* 2024; 25: 888–900.
- Taylor MH, Lee C-H, Makker V, et al. Phase IB/II Trial of Lenvatinib Plus Pembrolizumab in Patients With Advanced Renal Cell Carcinoma, Endometrial Cancer, and Other Selected Advanced Solid Tumors. *J Clin Oncol.* 2020; 38: 1154–63.
- Adkins D, Mehan P, Ley J, et al. Pazopanib plus cetuximab in recurrent or metastatic head and neck squamous cell carcinoma: an open-label, phase 1b and expansion study. *Lancet Oncol.* 2018; 19: 1082–93.
- Li X, Wang C, Zhang H, et al. circFND3B Accelerates Vasculature Formation and Metastasis in Oral Squamous Cell Carcinoma. *Cancer Res.* 2023; 83: 1459–75.
- Liu W, Ding Z, Tao Y, et al. A positive feedback loop between PFKP and c-Myc drives head and neck squamous cell carcinoma progression. *Mol Cancer.* 2024; 23: 141.
- Ludwig N, Yerneni SS, Azambuja JH, et al. TGFβ+ small extracellular vesicles from head and neck squamous cell carcinoma cells reprogram macrophages towards a pro-angiogenic phenotype. *J Extracell Vesicles.* 2022; 11: e12294.
- Li X, Jiang E, Zhao H, et al. Glycometabolic reprogramming-mediated proangiogenic phenotype enhancement of cancer-associated fibroblasts in oral squamous cell carcinoma: role of PGC-1α/PFKFB3 axis. *Br J Cancer.* 2022; 127: 449–61.
- Wang X, Zhao H, Luo X, et al. NNMT switches the proangiogenic phenotype of cancer-associated fibroblasts via epigenetically regulating ETS2/VEGFA axis. *Oncogene.* 2024; 43: 2647–60.
- Lee T-L, Chen T-H, Kuo Y-J, Lan H-Y, Yang M-H, Chu P-Y. Tumor-associated tissue eosinophilia promotes angiogenesis and metastasis in head and neck squamous cell carcinoma. *Neoplasia.* 2023; 35: 100855.
- Bates SE. Epigenetic Therapies for Cancer. *N Engl J Med.* 2020; 383: 650–63.
- Chen T, Dent SYR. Chromatin modifiers and remodellers: regulators of cellular differentiation. *Nat Rev Genet.* 2014; 15: 93–106.
- Resar L, Chia L, Xian L. Lessons from the Crypt: HMGA1-Amping up Wnt for Stem Cells and Tumor Progression. *Cancer Res.* 2018; 78: 1890–7.
- Bustin M. Regulation of DNA-dependent activities by the functional motifs of the high-mobility-group chromosomal proteins. *Mol Cell Biol.* 1999; 19: 5237–46.
- Chia L, Wang B, Kim J-H, et al. HMGA1 induces FGF19 to drive pancreatic carcinogenesis and stroma formation. *J Clin Invest.* 2023; 133: e151601.
- Li L, Kim J-H, Lu W, et al. HMGA1 chromatin regulators induce transcriptional networks involved in GATA2 and proliferation during MPN progression. *Blood.* 2022; 139: 2797–815.
- Hou P, Meng S, Li M, et al. LINC00460/DHX9/IGF2BP2 complex promotes colorectal cancer proliferation and metastasis by mediating HMGA1 mRNA stability depending on m6A modification. *J Exp Clin Cancer Res.* 2021; 40: 52.
- Liu M-J, Zhao Y, Li Q-T, et al. HMGA1 promotes the progression of esophageal squamous cell carcinoma by elevating TKT-mediated upregulation of pentose phosphate pathway. *Cell Death Dis.* 2024; 15: 541.
- Yang J-Y, Lei X-Y, He K-Y, et al. HMGA1 drives chemoresistance in esophageal squamous cell carcinoma by suppressing ferroptosis. *Cell Death Dis.* 2024; 15: 158.
- Que T, Zheng H, Zeng Y, et al. HMGA1 stimulates MYH9-dependent ubiquitination of GSK-3β via PI3K/Akt/c-Jun signaling to promote malignant progression and chemoresistance in gliomas. *Cell Death Dis.* 2021; 12: 1147.
- Tang C, Lei X, Xiong L, Hu Z, Tang B. HMGA1B/2 transcriptionally activated-POU1F1 facilitates gastric carcinoma metastasis via CXCL12/CXCR4 axis-mediated macrophage polarization. *Cell Death Dis.* 2021; 12: 422.
- Rho YS, Lim YC, Park IS, et al. High mobility group HMGI(Y) protein expression in head and neck squamous cell carcinoma. *Acta Otolaryngol.* 2007; 127: 76–81.
- Zhang YL, Song XF, Duan YJ, Zhao RL. [Expression and correlation of Fra-1 and HMGA1 in laryngeal squamous cell carcinoma]. *Zhonghua Er Bi Yan Hou Tou Jing Wai Ke Za Zhi.* 2017; 52: 927–32.
- Wang D-S, Pan C-C, Lai H-C, Huang J-M. Expression of HMGA1 and ezrin in laryngeal squamous cell carcinoma. *Acta Otolaryngol.* 2013; 133: 626–32.
- Sterenczak KA, Eckardt A, Kampmann A, et al. HMGA1 and HMGA2 expression and comparative analyses of HMGA2, Lin28 and let-7 miRNAs in oral squamous cell carcinoma. *BMC Cancer.* 2014; 14: 694.
- Miyazawa J, Mito A, Kawashiri S, Chada KK, Imai K. Expression of mesenchyme-specific gene HMGA2 in squamous cell carcinomas of the oral cavity. *Cancer Res.* 2004; 64: 2024–9.
- Palumbo A, De Martino M, Esposito F, et al. HMGA2, but not HMGA1, is overexpressed in human larynx carcinomas. *Histopathology.* 2018; 72: 1102–14.
- Larsson L, Jäwert F, Magnusson B, Hasséus B, Kjeller G. Expression of high mobility group A proteins in oral leukoplakia. *Anticancer Res.* 2013; 33: 4261–6.
- Yu C-H, Hsieh P-L, Chao S-C, Chen S-H, Liao Y-W, Yu C-C. XIST/let-7i/HMGA1 axis maintains myofibroblasts activities in oral submucous fibrosis. *Int J Biol Macromol.* 2023; 232: 123400.
- Zanin R, Pegoraro S, Ros G, et al. HMGA1 promotes breast cancer angiogenesis supporting the stability, nuclear localization and transcriptional activity of FOXM1. *J Exp Clin Cancer Res.* 2019; 38: 313.
- Di Cello F, Hillion J, Kowalski J, et al. Cyclooxygenase inhibitors block uterine tumorigenesis in HMGA1a transgenic mice and human xenografts. *Mol Cancer Ther.* 2008; 7: 2090–5.
- Hu Y, Smyth GK. ELDA: extreme limiting dilution analysis for comparing depleted and enriched populations in stem cell and other assays. *J Immunol Methods.* 2009; 347: 70–8.
- Czubayko F, Liaudet-Coopman ED, Aigner A, Tuveson AT, Berchem GJ, Wellstein A. A secreted FGF-binding protein can serve as the angiogenic switch in human cancer. *Nat Med.* 1997; 3: 1137–40.
- Shintani T, Higaki M, Okamoto T. Heparin-Binding Protein 17/Fibroblast Growth Factor-Binding Protein-1 Knockout Inhibits Proliferation and Induces Differentiation of Squamous Cell Carcinoma Cells. *Cancers (Basel).* 2021; 13: 2684.
- Rosli SNZB, Shintani T, Toratani S, Usui E, Okamoto T. 1α,25(OH)₂D₃ inhibits FGF-2 release from oral squamous cell carcinoma cells through down-regulation of HBp17/FGFBP-1. *In vitro Cell Dev Biol Anim.* 2014; 50: 802–6.
- Lee C, Chen R, Sun G, et al. VEGF-B prevents excessive angiogenesis by inhibiting FGF2/FGFR1 pathway. *Signal Transduct Target Ther.* 2023; 8: 305.
- Begum S, Zhang Y, Shintani T, Toratani S, Sato JD, Okamoto T. Immunohistochemical expression of heparin-binding protein 17/fibroblast growth factor-binding protein-1 (HBp17/FGFBP-1) as an angiogenic factor in head and neck tumorigenesis. *Oncol Rep.* 2007; 17: 591–6.
- Li W, Wang C, Juhn SK, Ondrey FG, Lin J. Expression of fibroblast growth factor binding protein in head and neck cancer. *Arch Otolaryngol Head Neck Surg.* 2009; 135: 896–901.
- Vellucci VF, Germino FJ, Reiss M. Cloning of putative growth regulatory genes from primary human keratinocytes by subtractive hybridization. *Gene.* 1995; 166: 213–20.
- Li G, Oparil S, Kelpke SS, Chen Y-F, Thompson JA. Fibroblast growth factor receptor-1 signaling induces osteopontin expression and vascular smooth muscle cell-dependent adventitial fibroblast migration *in vitro*. *Circulation.* 2002; 106: 854–9.
- Calandrella N, Risuleo G, Scarsella G, et al. Reduction of cell proliferation induced by PD166866: an inhibitor of the basic fibroblast growth factor. *J Exp Clin Cancer Res.* 2007; 26: 405–9.
- Risuleo G, Ciacciarelli M, Castelli M, Galati G. The synthetic inhibitor of fibroblast growth factor receptor PD166866 controls negatively the growth of tumor cells in culture. *J Exp Clin Cancer Res.* 2009; 28: 151.
- Okuyama K, Naruse T, Yanamoto S. Tumor microenvironmental modification by the current target therapy for head and neck squamous cell carcinoma. *J Exp Clin Cancer Res.* 2023; 42: 114.

48. Chu X, Tian W, Ning J, et al. Cancer stem cells: advances in knowledge and implications for cancer therapy. *Signal Transduct Target Ther.* 2024; 9: 170.
49. Lugli A, Zlobec I, Berger MD, Kirsch R, Nagtegaal ID. Tumour budding in solid cancers. *Nat Rev Clin Oncol.* 2021; 18: 101-15.
50. Wang W, Yun B, Hoyle RG, et al. CYTOR Facilitates Formation of FOSL1 Phase Separation and Super Enhancers to Drive Metastasis of Tumor Budding Cells in Head and Neck Squamous Cell Carcinoma. *Adv Sci (Weinh).* 2024; 11: e2305002.
51. Alessandrini L, Astolfi L, Daloiso A, et al. Diagnostic, Prognostic, and Therapeutic Role for Angiogenesis Markers in Head and Neck Squamous Cell Carcinoma: A Narrative Review. *Int J Mol Sci.* 2023; 24: 10733.
52. Saba NF, Vijayvargiya P, Vermorken JB, et al. Targeting Angiogenesis in Squamous Cell Carcinoma of the Head and Neck: Opportunities in the Immunotherapy Era. *Cancers (Basel).* 2022; 14: 1202.